Multilayer mirrored bubbles with spatially-chirped and elastically-tuneable optical bandgaps

Gen Kamita,[1] Mathias Kolle,[2] Fumin Huang,[1] Jeremy J. Baumberg,[1*] and Ullrich Steiner[1,*]

[1]*Cavendish Laboratory, University of Cambridge, Cambridge, CB3 0HE, UK*
[2]*School of Engineering and Applied Sciences, Harvard University, Cambridge 02138, USA*
[*]*u.steiner@phy.cam.ac.uk*

Abstract: We demonstrate the multifolding Origami manufacture of elastically-deformable Distributed Bragg Reflector (DBR) membranes that reversibly color-tune across the full visible spectrum without compromising their peak reflectance. Multilayer films composed of alternating transparent rubbers are fixed over a 300 μm wide pinhole and deformed by pressure into a concave shape. Pressure-induced color tuning from the near-IR to the blue arises from both changes in thickness of the constituent layers and from tilting of the curved DBR surfaces. The layer thickness and color distribution upon deformation, the band-gap variation and the repeatability of cyclic color tuning, are mapped through micro-spectroscopy. Such spatially-dependent thinning of the film under elastic deformation produces spatial chirps in the color, and are shown to allow reconstruction of complex 3D strain distributions.

© 2012 Optical Society of America

OCIS codes: (220.4241) Nanostructure fabrication; (230.1480) Bragg reflectors; (350.4238) Nanophotonics and photonic crystals.

References and links

1. U. Scherf, "Conjugated polymers: lasing and stimulated emission," Curr. Opin. Solid State Mater. Sci. **5**, 143–154 (2001).
2. X. Xu, Y. Dai, X. Chen, D. Jiang, and S. Xie, "Chirped and phase-sampled fiber bragg grating for tunable dbr fiber laser," Opt. Express **13**, 3877–3882 (2005).
3. T. Komikado, a. Inoue, K. Masuda, T. Ando, and S. Umegaki, "Multi-layered mirrors fabricated by spin-coating organic polymers," Thin Solid Films **515**, 3887–3892 (2007).
4. Y. Yang, G. A. Turnbull, and I. D. W. Samuel, "Hybrid optoelectronics: A polymer laser pumped by a nitride light-emitting diode," Appl. Phys. Lett. **92**, 163306 (2008).
5. K. D. Singer, T. Kazmierczak, J. Lott, H. Song, Y. Wu, J. Andrews, E. Baer, A. Hiltner, and C. Weder, "Melt-processed all-polymer distributed bragg reflector laser," Opt. Express **16**, 10358–10363 (2008).
6. A. Y. Cho, G. J. Zydzik, E. F. Schubert, Y.-H. Wang, and L.-W. Tu, "Resonant cavity light-emitting diode," Appl. Phys. Lett. **60**, 921–923 (1992).
7. S. Chang, C. Chang, Y. Su, P. Chang, Y. Wu, K. Huang, and T. Chen, "Chirped GaAs-AlAs distributed Bragg reflectors for high brightness yellow-green light-emitting diodes," IEEE Photon. Technol. Lett. **9**, 182–184 (1997).
8. S. W. Chiou, C. P. Lee, C. K. Huang, and C. W. Chen, "Wide angle distributed Bragg reflectors for 590 nm amber AlGaInP light-emitting diodes," J. Appl. Phys. **87**, 2052–2054 (2000).
9. Y. Kang, J. Walish, T. Gorishnyy, and E. Thomas, "Broad-wavelength-range chemically tunable block-copolymer photonic gels," Nat. Mater. **6**, 957–960 (2007).
10. S. Colodrero, M. Ocaña, and H. Míguez, "Nanoparticle-based one-dimensional photonic crystals," Langmuir **24**, 4430–4434 (2008).

#161038 - $15.00 USD Received 12 Jan 2012; revised 10 Feb 2012; accepted 13 Feb 2012; published 5 Mar 2012
(C) 2012 OSA

11. O. Sánchez-Sobrado, M. Calvo, N. Núñez, M. Ocaña, G. Lozano, and H. Míguez, "Environmentally responsive nanoparticle-based luminescent optical resonators," Nanoscale **2**, 936–941 (2010).
12. S. Guldin, M. Kolle, M. Stefik, R. Langford, D. Eder, U. Wiesner, and U. Steiner, "Tunable mesoporous bragg reflectors based on block-copolymer self-assembly," Adv. Mater. **23**, 3664–3668 (2011).
13. S. Colodrero, A. Mihi, L. Häggman, M. Ocaña, G. Boschloo, A. Hagfeldt, and H. Míguez, "Porous one-dimensional photonic crystals improve the power-conversion efficiency of dye-sensitized solar cells," Adv. Mater. **21**, 764–770 (2009).
14. S. Colodrero, A. Mihi, J. a. Anta, M. Ocaña, and H. Míguez, "Experimental demonstration of the mechanism of light harvesting enhancement in photonic-crystal-based dye-sensitized solar cells," J. Phys. Chem. C **113**, 1150–1154 (2009).
15. M. E. Calvo and H. Míguez, "Flexible, adhesive, and biocompatible Bragg mirrors based on polydimethylsiloxane infiltrated nanoparticle multilayers," Chem. Mater. **22**, 3909–3915 (2010).
16. M. H. Song, B. Wenger, and R. H. Friend, "Tuning the wavelength of lasing emission in organic semiconducting laser by the orientation of liquid crystalline conjugated polymer," J. Appl. Phys. **104**, 033107 (2008).
17. M. Kolle, P. M. Cunha, M. R. J. Scherer, H. Fumin, P. Vukusic, S. Mahajan, J. Baumberg, and U. Steiner, "Mimicking the colourful wing scale structure of the Papilio blumei butterfly," Nat. Nanotechnol. **5**, 511–515 (2010).
18. A. Hotta, S. M. Clarke, and E. M. Terentjev, "Stress relaxation in transient networks of symmetric triblock styrene-isoprene-styrene copolymer," Macromolecules **35**, 271–277 (2002).
19. S. Coyle, G. V. Prakash, J. J. Baumberg, M. Abdelsalem, and P. N. Bartlett, "Spherical micromirrors from templated self-assembly: Polarization rotation on the micron scale," Appl. Phys. Lett. **83**, 767–769 (2003).
20. P. Vukusic, J. R. Sambles, and C. R. Lawrence, "Colour mixing in wing scales of a butterfly," Nature **404**, 457 (2000).
21. P. Vukusic, R. Sambles, C. Lawrence, and G. Wakely, "Sculpted-multilayer optical effects in two species of Papilio butterfly," Appl. Optics **40**, 1116–1125 (2001).
22. S. Yoshioka and S. Kinoshita, "Polarization-sensitive color mixing in the wing of the madagascan sunset moth," Opt. Express **15**, 2691–2701 (2007).
23. M. Kolle, B. Zheng, N. Gibbons, J. J. Baumberg, and U. Steiner, "Stretch-tuneable dielectric mirrors and optical microcavities," Opt. Express **18**, 575–581 (2010).
24. J. Zhu, S. Cai, and Z. Suo, "Resonant behavior of a membrane of a dielectric elastomer," Int. J. Solids Struct. **47**, 3254–3262 (2010).
25. S.-H. Yoon, V. Reyes-Ortiz, K.-H. Kim, Y. H. Seo, and M. R. K. Mofrad, "Analysis of circular PDMS microballoons with ultralarge deflection for MEMS design," J. Microelectromech. S **19**, 854–864 (2010).

1. Introduction

Distributed Bragg reflectors (DBRs), are used as spectrally selective mirrors in many different optical systems, including lasers [1–5], light emitting diodes (LEDs) [6–8] sensing [9–12] and photovoltaics [13–15]. The realization of a band-gap elastic DBR provides opportunities for the development of novel emission devices such as tunable lasing [16,17] or LED [17] systems, and mechanical sensing devices such as pressure or acoustic sensors. In this article we demonstrate the manufacture of highly-flexible DBR membranes that exhibit a high reflectance stop-band. The stop-band center can be tuned from 830 nm in the near-IR down to 400 nm in the blue, without compromising the reflection intensity. Simple color-tuning is achieved by pressurising elastic multilayer membranes stretched over a pinhole, deforming them into spherical shapes. Detailed spatially-resolved spectroscopy allows analysis of the color variation across such concavely deformed DBRs, the polarization rotation observed when light reflects off curved regions, and the spatial distribution of the film thickness of the deformed multilayer. Such films can thus be used to analyse the strain distribution in complex deformations of 3D objects.

2. Materials and methods

2.1. Fabrication of the elastic DBR

Elastic DBRs were assembled starting from an elastic bilayer, employing an 'Origami' folding technique (Fig. 1), which improves over earlier approaches [17]. A thin polysulfonic acid (PSS) layer was first spin-cast onto a silicon wafer. The PSS layer is marked with a set of orthogonal

#161038 - $15.00 USD Received 12 Jan 2012; revised 10 Feb 2012; accepted 13 Feb 2012; published 5 Mar 2012
(C) 2012 OSA

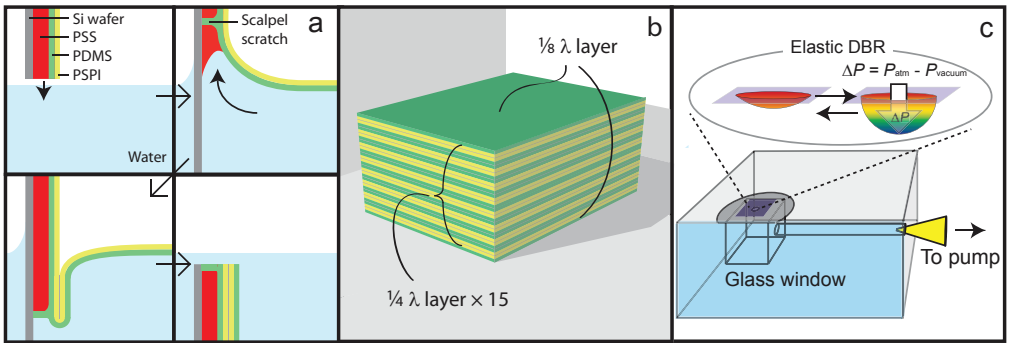

Fig. 1. (a) Illustration of the Origami technique. The elastic DBR is assembled by immersing the Si wafer coated with a PSS-PDMS-PSPI trilayer into water. The PDSM-PSPI double layer floats onto the water surface by dissolving an underlying PSS layer until it reaches a scratch in the PSS film, stopping PSS dissolution. Further immersion causes the PDMS-PSPI bilayer to fold back to the upper half of the wafer. The folding steps completes by full submersion of the wafer. (b) Elastic DBR after 4 folding steps. (c) Illustration of the home-made sample holder supporting an elastic DBR over a pinhole.

scratches which extend down to the substrate. A 90 nm thick polydimethyl siloxane (PDMS, Dow Corning - Sylgard 184) film was then cast from heptane solution onto the PSS layer followed by cross-linking at 120 °C for one hour. Polystyrene-polyisoprene triblock terpolymer (PSPI, Sigma Aldrich) was subsequently cast from toluene onto the insoluble PDMS rubber to form a 60 nm thick layer. The supported trilayer sample was then immersed into water, dissolving the PSS, which causes the PDMS-PSPI layer to float onto the top water surface. PSS dissolution stops as soon as the water reaches one of the scalpel scratches, where the PDMS is pinned to the substrate surface . Continued immersion of the substrate into the water forces the bilayer to fold back onto the upper-half of the substrate, forming a U-fold of the bilayer (Fig. 1(a)). The sample was then rotated by 90° and the immersion process repeated. Repeating the folding steps 5 or 6 times results in multilayers comprising 31 or 63 stacked alternating PDMS and PSPI films of double the thickness compared to the initial spin-cast thickness. The number of the PDMS and PSPI double layers, n, is given by

$$n = 2^m - 1 \tag{1}$$

where m is the number of the folding steps. The outmost PDMS single layers are not included in this layer number because they do not contribute to the DBR interference (Fig. 1(b)). The final resulting multilayers have low defect density. Given the refractive indices of 1.41 and 1.53 for PDMS and PSPI, respectively, the resulting multilayer stack forms a DBR with a stop band that is centred in the infrared at $\sim$ 800 nm, with a stop-band reflectance of around 80%.

2.2. *Actuation of elastic DBRs*

The DBR multilayers were floated onto thin stainless steel sheets containing a 300 µm-wide pinhole. A 63 layer-containing DBR was employed for full color actuation tests, while further spectroscopy was performed on DBRs comprising 31 layers. The pinholed sheet was fixed air-tight onto a channel in a transparent plexiglass holder (Fig. 1(c)) and the channel connected to a pump and a pressure gauge, allowing variable evacuation of the volume under the pinhole. A pressure difference established across the air-impermeable multilayer membrane leads to an elastic deformation of the DBR into a concave shape. The degree of deformation was controlled by adjusting the pressure difference up to a maximum $\Delta P = 0.33$ bar. The DBR membrane was

#161038 - $15.00 USD Received 12 Jan 2012; revised 10 Feb 2012; accepted 13 Feb 2012; published 5 Mar 2012
(C) 2012 OSA

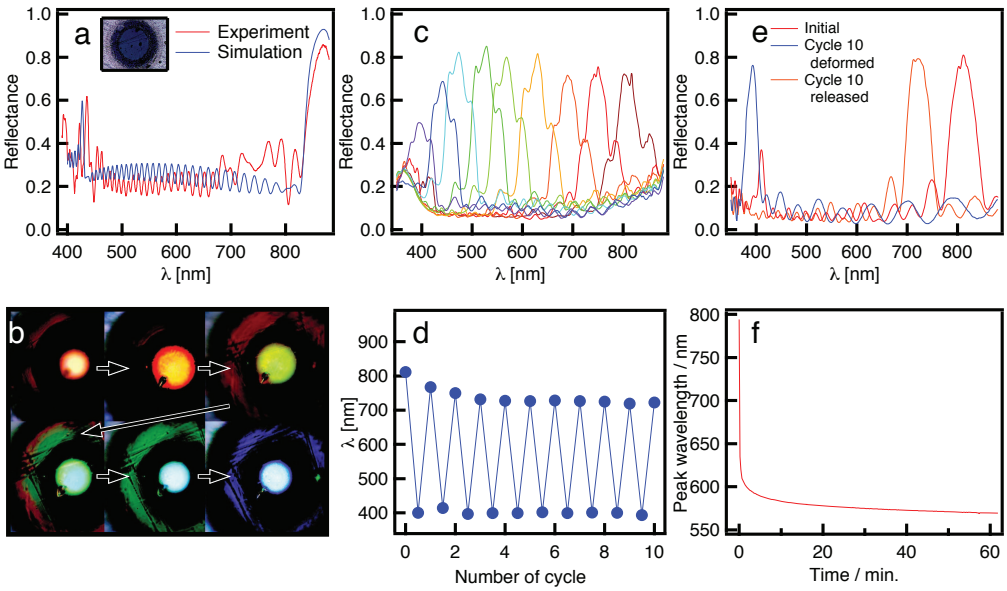

Fig. 2. (a) Experimental and simulated reflection spectra of a flat elastic DBR still attached to its Si substrate. Simulation parameters were $d_{\mathrm{PDMS}} = 175\,\mathrm{nm}$, $d_{\mathrm{PSPI}} = 123\,\mathrm{nm}$, $n_{\mathrm{PDMS}} = 1.41$, and $n_{\mathrm{PSPI}} = 1.53$. The inset shows an elastic DBR on a 300 μm-wide pinhole in its initial flat state. (b) A deformed DBR under increasing pressure showing color shifts from red (top left) to blue (bottom right). (c) Reflection spectra taken during actuation showing shift of stop-band to 400 nm with pressure difference $\Delta P = 0.33$ bar. (d,e) Stop-band tuning of the DBR performed over ten cycles by repeatedly switching ΔP between 0 to 0.32 bar. (f) Peak reflectance position extracted from a time resolved spectral measurement after pressure difference was increased to $\Delta P = 0.25$ bar.

observed by microscopy and confocal micro-spectroscopy throughout deformation and optical micrographs of the deformed DBR taken in top- and side-view. The profile of the deformed DBR extracted from side view images provides access to the shape of the film deformation. In all cases a spherical curvature of the DBR membranes was found. For transmission spectroscopy and curvature evaluation, the deformed DBR was kept under a constant pressure difference for approximately 10 minutes before the measurement in order to allow the deformed state to equilibrate.

3. Results

3.1. Full color DBR tuning

Images of the DBR membrane under deformation show a change in hue from red to blue (Fig. 2(a) and 2(b)). Reflection spectra from the cavity center reveal the dependence of the stop-band peak wavelength on the applied deformation. The stop-band peak smoothly shifts from 800 nm in the near-IR to 400 nm in the blue without a variation in peak intensity (Fig. 2(c)). This indicates that the ratio of thicknesses of the PDMS and PSPI layers in the DBR remains constant with increasing strain, which is the consequence of equal Poisson ratios of the two elastic layers.

The change in peak reflectance wavelength induced by a variation in light incidence angle

#161038 - $15.00 USD Received 12 Jan 2012; revised 10 Feb 2012; accepted 13 Feb 2012; published 5 Mar 2012
(C) 2012 OSA

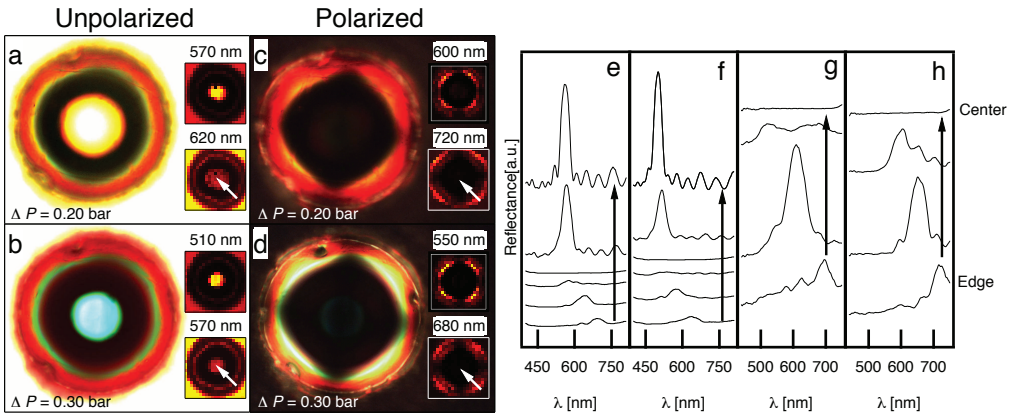

Fig. 3. (a-d) Observation of rotation by polarization microscopy and micro spectroscopy. Images of the deformed DBR, both (a,b) without and (c,d) with crossed polarizers for (a,c) $\Delta P = 0.20$, (b,d) $\Delta P = 0.30$. Optical reflection from the center is blocked by the crossed polarizer while regions near the rim remain bright, which is characteristic for a polarization rotation by double reflection. The insets show images at the indicated wavelengths. (e-h) reflectance along the path indicated by the arrows in (a-d), respectively.

and layer thickness upon deformation follows the simple relation

$$m\lambda/2 = d_1\sqrt{n_1^2 - \sin^2\theta} + d_2\sqrt{n_2^2 - \sin^2\theta} \tag{2}$$

where d_1, d_2, n_1 and n_2 are the thicknesses and the refractive indices of the two multilayer materials, θ is the incident angle of the light and m is a natural number. Analysis of these data reveals a decrease in thickness to one-half of the unstrained value for $\Delta P = 0.33$ bar.

A cyclic tuning test was performed in order to demonstrate the repeatability of stop-band tuning. The elastic DBR peak wavelength was tuned from a starting value of ~800 nm to 400 nm and back for 10 cycles (Fig. 2(d)). Although a reflectance at 400 nm was attained a few seconds after turning on the vacuum pump, returning to ambient pressure did not lead to immediate restoration of the membrane to its original color. The layer was allowed to relax for 5 minutes before starting the next cycle to allow the reflection peak wavelength to recover beyond 700 nm. The reflection intensities remained stable throughout the 10 cycles of tuning (Fig. 2(e)).

A time resolved spectral measurement was performed after applying a fixed pressure difference of $\Delta P = 0.25$ bar. The peak reflectance shifted from 800 to 600 nm during the initial 100 seconds, followed by a gradual shift to 570 nm over the following hour. This is indicative of a viscoelastic behavior of the rubber film. While every rubber shows viscoelasticity to a small degree, it is likely that the substantial creep of Fig. 2(f) is dominated by the PSPI layer. In contrast to the chemical cross-links of the cured PDMS layer, PSPI forms physical cross-links by PS micro-phase separation which have been shown to enable creep at temperatures above 30° C, where chain pull-out and PS reassembly take place if a sufficiently high force is applied [18]. This behavior is likely to affect the recovery speed upon elastic deformation. One possible way to overcome this is to use a polymer with similar optical properties (e.g. pure polyisoprene) that can be chemically cross-linked.

3.2. Polarization rotation

Polarization rotation by the pressure-deformed DBR was observed in a microscope with two crossed polarizers (Fig. 3(a)-3(d)). Light incident off-centre onto the concave multilayer sur-

#161038 - $15.00 USD Received 12 Jan 2012; revised 10 Feb 2012; accepted 13 Feb 2012; published 5 Mar 2012
(C) 2012 OSA

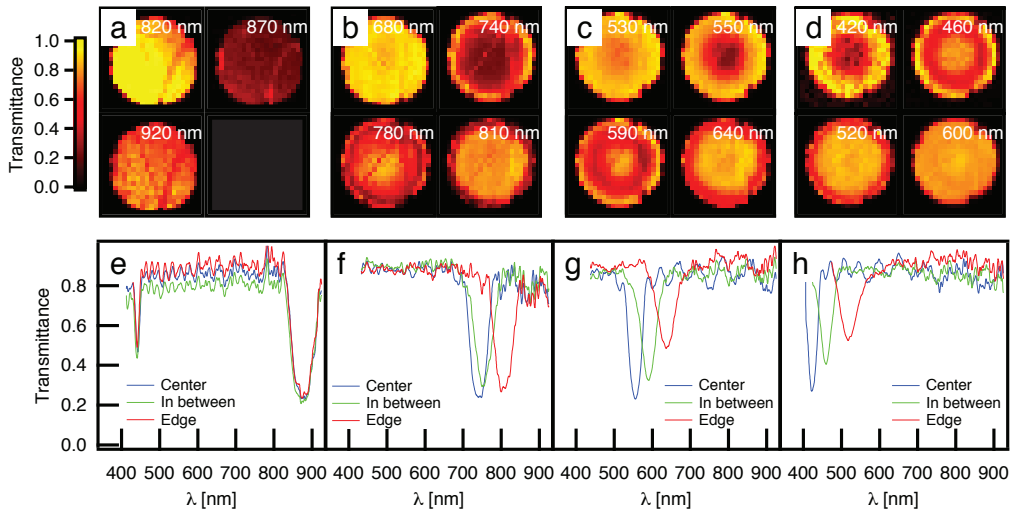

Fig. 4. (a-d) Spatial distribution of transmitted intensity at different wavelengths. The maps were taken (a) in the initial non-deformed state, (b) the residual concavity state after deformation and relaxation, (c) $\Delta P = 0.17$ bar and (d) $\Delta P = 0.27$ bar. (e-h) Spectra extracted from (a-d), respectively. The small red shift in (f) is due to the permanent deformation of the multilayer after actuation.

face can undergo more than one reflection within the concavity. Multiple bounces within the concavity induce a polarization rotation caused by a different overall phase shift between TE- and TM-polarized reflections, compared to singly-reflected light. Previous studies have demonstrated that light reflected from hemispherical metal mirrors [19] and from the photonic structures on butterfly and moth wing scales give rise to a similar effect [20–22]. Concave cuticle-air mutlilayers on the wings scales of *Papilio blumei* cause polarization rotation for blue light after a double bounce from the concavity edges [20, 23]. Observation of the concavities between crossed polarizers suppresses the yellow center reflection, rendering the butterfly scales macroscopically blue.

Similar to *Papilio blumei*, the deformed DBR shows a difference in color between the center and the edge of the bubble DBR. The double bounce reflection of light from the cavity edges is revealed by the observed differences in reflection color with and without crossed polarizers which is characteristic for *Papillo*-like polarization rotation. Interestingly, light reflected from the center of the deformed rubber DBR is blue-shifted compared to the edge reflection (Fig. 3(a) and 3(b)), in contrast to *Papillo* scale where the center reflection is red-shifted. This microscopic observation is confirmed by the spectra (Fig. 3(e)-3(h)) which show a clear blue shift of the center stop-band peak. This observation is seemingly in contradiction with Eq. (2) which predicts a red shift of the center reflection compared to the concavity edges. The reason for this inverted colour performance for the elastic DBR is a systematic variation in PDMS and PSPI layer thickness in the center compared to the edges upon deformation, resulting in a net red-shift. This shift to shorter wavelengths from the edges to the center therefore indicates a higher local strain of the polymer layers at the concavity center, as discussed below.

3.3. Spatial chirp

In order to confirm a radially inhomogeneous strain distribution within the concavely shaped DBR, the sample was mapped spectroscopically in transmission with a resolution of 15 µm

#161038 - $15.00 USD Received 12 Jan 2012; revised 10 Feb 2012; accepted 13 Feb 2012; published 5 Mar 2012
(C) 2012 OSA

(Fig. 4). The elastic DBR in its non-deformed state has a homogeneous stop-band distribution (Fig. 4(a) and 4(e)). At $\Delta P = 0$ after several actuation steps, it acquires slight permanent concave form caused by the repeated tuning cycles. The spectrum taken at the center of the pinhole shows a stop-band around 745 nm, compared to a stop-band peak of ~ 800 nm at the concavity edge (Fig. 4(b) and 4(f)). This is a clear indication of localized film thinning at the center. The red shift becomes more pronounced when the elastic DBR is further deformed, with a stop-band difference of up to 100 nm (Fig. 4(d) and 4(h)).

Further evidence of the localized thinning was acquired by analyzing the film radial thickness distribution. Micrographs taken through the side window of the custom-made sample holder revealed the change in the curvature of the deformed multilayer for increasing pressure differences (Fig. 5(a)-5(c)). The variation of incident angles across the spherically deformed DBR membrane were calculated from the shape of the deformed DBR. The thickness distribution along the deformed DBR as a function of horizontal distance from the pinhole center was then calculated using Eq. (1) with λ acquired from the spectral maps and θ from angle distribution maps (Fig. 5(d)). The initial elastic DBR before actuation has a homogeneous thickness distribution. The hemispherical geometry of the actuated film concentrates the strain at the center, thereby enhancing the observed spectral shift.

The spherical nature of the shape is further revealed when plotting the relative thickness against the local deflection at different radial positions (Fig. 5(e)). Although the actual shape of such an elastic bubble is a highly complicated non-analytic function, as the pressure increases the bubble shape becomes more spherical and the thickness directly tracks the deflection [24]. This can also be seen in the linearity of the maximum strain found at the centre of the membrane with the local deflection at that point (Fig. 5(f)). These features point to the robustly predictable nature of suitable designed elastomeric optical components. Extraction of such data on deformed membranes has been previously difficult, and the use optically-functional membranes opens up new capabilities for understanding 3D elastic deformations in detail.

Such non-uniform strain distributions suggest a new route to spectroscopic components. Combining such non-uniformly strained dielectric multilayers yielding chirped thickness variations together with diode arrays and CCDs, allows reconfigurable hyperspectral imaging. While the demonstration shown here was of a regularly-spaced DBR, the complete range of multilayer

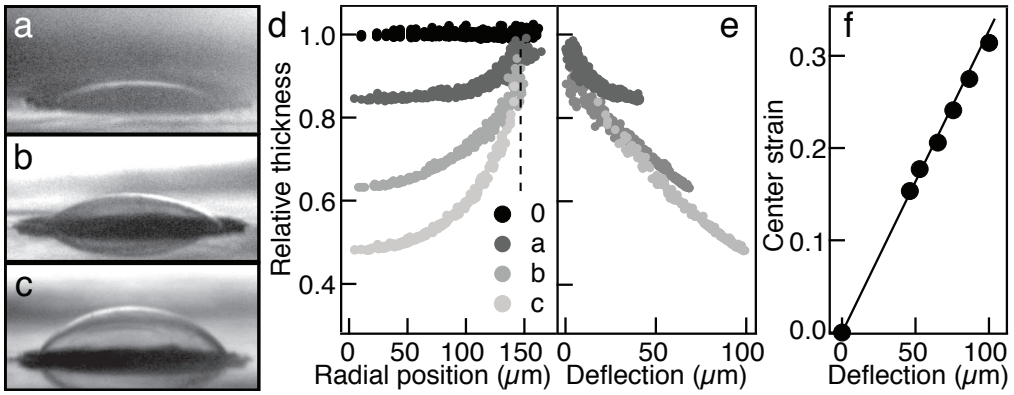

Fig. 5. (a-c) Images of a deformed DBR taken in the permanently deformed state, and with applied pressures of 0, 0.17 and 0.27 bar. (d) PDMS and PSPI layer thickness variation of the elastic DBR across the pinhole extracted from the spectral maps, together with (e) its dependence on the local deflection. (f) Extracted strain at the mirror centre *vs* the deflection produced by different pressures.

#161038 - $15.00 USD Received 12 Jan 2012; revised 10 Feb 2012; accepted 13 Feb 2012; published 5 Mar 2012
(C) 2012 OSA

filter functions are possible, including high-pass, low-pass, bandpass, notch and dichroic elements. Applications include Raman edge filters for maximising laser rejection by elastic tuning, as well as graded photonic bandgap systems useful for adjustable negative dispersions for pulse compression. Improvements require control of the creep identified in such systems, through better control of the cross-linking.

4. Conclusion

We have demonstrated the repeatable full color tuning of elastically deformable DBRs across the entire optical spectrum without compromising the peak reflectance. Light reflected from the edge of the deformed DBRs showed polarization rotation, while the center reflection was blue shifted compared to the edge. These effects are caused by multiple reflection of incident light at the edge and localized film thinning at the center of the deformed DBRs.

Future developments will allow acquisition of thickness and curvature data from the elastic DBR to allow extention of this work to the study of inflation of micro-balloons [25]. Such structures also provide prospects for the development of color displays, resonant cavities for tunable lasing, tunable LEDs, and bio-inspired filters/reflectors for security applications. Using chemically cross-linked polyisoprene instead of PSPI should enhance actuation sensitivity and decrease the response time to pressure changes, enabling the development of accurate low-cost optical acoustic sensors.

Acknowledgments

This work was supported by EPSRC EP/G060649/1.

#161038 - $15.00 USD Received 12 Jan 2012; revised 10 Feb 2012; accepted 13 Feb 2012; published 5 Mar 2012
(C) 2012 OSA